

An efficient sensitivity analysis for optimal 3D deformation process design

Nicholas Zabaras and Swagato Acharjee

Materials Process Design and Control Laboratory, Sibley School of Mechanical and Aerospace Engineering, 188 Frank H.T. Rhodes Hall, Cornell University, Ithaca, NY 14853-3801, USA

Abstract: In this work, we present a gradient optimization technique for optimizing deformation processes. The optimization is based on the continuum sensitivity method (CSM). CSM involves differentiation of the governing field equations of the direct problem (constitutive, contact and kinematic problems) with respect to the design variables and development of the weak forms for the corresponding continuum sensitivity equations. The present 3D developments involve a novel regularized approach to the contact sensitivity problem that addresses the non-differentiability of the contact constraints. A relevant 3D die design problem and a 3D preform design problem are considered highlighting the features of the algorithm developed.

1. Introduction: Though there has been extensive work by different groups in simulating the direct problem in forming processes, comparatively less attention has been devoted in developing a strategy for solving the design problems that arise in this field. As a result most of the methods for industrial deformation process design are currently focused on trial and error techniques. In this paper, we have developed an algorithm for metal forming design based on a gradient optimization framework. The gradients of the objective function are calculated using the sensitivity fields obtained from the finite element implementation of the continuum sensitivity method (CSM). The continuum equations defining the sensitivity fields in the CSM are obtained by design-differentiating (i.e. differentiating with respect to the design variables) the continuum governing equations of the direct problem. The finite element form of the CSM is posed by introducing an appropriate weak form of the continuum sensitivity equations and subsequent finite element discretization and approximation. This work is an extension of our previous work which was restricted to 2D applications [1]-[5]. Extending to 3D applications involves a new continuum sensitivity formulation of the contact problem based on the method suggested by Laursen in [6]. The 3D sensitivity contact subproblem is also defined in a fully continuum setting that allows us to accurately compute the sensitivities of the contact tractions as required by the sensitivity deformation problem.

2. The direct large deformation problem: A review of the direct deformation problem utilized in our design simulator is given in [1]-[4]. Let us denote with \mathbf{B}_0 the initial undeformed configuration of the body before any processing and with \mathbf{B}_n the configuration obtained at time t_n as a result of deformation processing.

The direct problem involves computing the time history of the deformation, temperature, material state and plastic deformation of a body deforming as a result of external forces and/or deformation due to contact and friction at the workpiece-die interface. The deformation problem is sub-divided into kinematic, constitutive, contact and thermal sub-problems. An updated Lagrangian FEM formulation is used to solve the direct deformation problem in a generic forming stage in which material occupying an initial configuration \mathbf{B}_0 is deformed to obtain a final configuration $\mathbf{B}_f(t = t_f)$. To compute the material configuration \mathbf{B}_{n+1} for $n = 0, 1, \dots, (f - 1)$, we proceed in an incremental fashion using the configuration \mathbf{B}_n as the reference configuration. Let \mathbf{X} be a material particle in \mathbf{B}_0 and let $\mathbf{x} = \tilde{\mathbf{x}}(\mathbf{X}, t)$ be its location at time t . The total deformation gradient can be defined as

$$\mathbf{F}(\mathbf{X}, t) = \nabla_0 \tilde{\mathbf{x}}(\mathbf{X}, t) = \frac{\partial \tilde{\mathbf{x}}(\mathbf{X}, t)}{\partial \mathbf{X}} \quad (1)$$

In the kinematic framework adopted for large deformation inelastic analysis including thermal effects, the total deformation gradient is decomposed into thermal, plastic and elastic parts as follows:

$$\mathbf{F} \equiv \mathbf{F}_{n+1} = \mathbf{F}^e \mathbf{F}^p \mathbf{F}^\theta \quad (2)$$

where \mathbf{F}^e is the elastic deformation gradient, \mathbf{F}^p , the plastic deformation gradient and \mathbf{F}^θ is the thermal part of the deformation gradient in \mathbf{B}_{n+1} . Using an updated Lagrangian framework, the total deformation gradient \mathbf{F}_{n+1} at time $t = t_{n+1}$ can be expressed in terms of \mathbf{F}_n at time $t = t_n$ as follows:

$$\mathbf{F}_{n+1} = \mathbf{F}_r \mathbf{F}^n \quad (3)$$

where \mathbf{F}_r is the relative deformation gradient. The equilibrium equation at $t = t_{n+1}$ can be expressed in the reference configuration \mathbf{B}_n as,

$$\nabla_n \bullet \mathbf{P}_r + f = 0 \quad (4)$$

where ∇_n denotes the divergence in \mathbf{B}_n and \mathbf{P}_r denotes the Piola-Kirchhoff I stress. The solution of the deformation problem in the current processing stage proceeds incrementally in time starting from the initial configuration \mathbf{B}_0 . In order to solve the equilibrium equation (Eq. (4)) at time $t = t_{n+1}$, the constitutive relationship between \mathbf{P}_r and the relative deformation gradient \mathbf{F}_r and temperature θ should be evaluated. State variable-based constitutive models have been used earlier in our work and details on the direct and sensitivity constitutive problems are not given here as the methodology is identical to

that used in our earlier 2D work in [1]. In extending the direct deformation problem to 3D, the kinematic and the thermal sub-problems are also mathematically identical to the developments in the 2D formulation. The contact sub-problem requires a different approach, which is discussed in detail in the following subsection.

2.1 Three dimensional implementation of the die-workpiece contact and frictional conditions: The contact and the friction model implemented is based on the implicit approach proposed in [6]. The schematic of the contact model is shown in Fig. 1. The die is assumed to be rigid and its surface is parameterized in three dimensions using the parameters $\xi = [\xi^1, \xi^2]$. Any point on the die can be represented as $\mathbf{y}(\xi) = (y_1(\xi), y_2(\xi), y_3(\xi))$, where $0 \leq \xi^1, \xi^2 \leq 1$. At each point of the die surface, we define a local basis with the tangent and the normal vectors at that point. The tangent vectors can be defined as follows:

$$\boldsymbol{\tau}_\alpha = \mathbf{y}_{,\xi^\alpha} = \frac{\partial y_1}{\partial \xi^\alpha} \mathbf{e}_1 + \frac{\partial y_2}{\partial \xi^\alpha} \mathbf{e}_2 + \frac{\partial y_3}{\partial \xi^\alpha} \mathbf{e}_3, \quad \alpha = 1, 2 \quad (5)$$

The unit normal at the same point can be defined as a cross product of the tangent vectors with unit norm. The die surface separates the continuum space into the admissible and the inadmissible regions. The region \mathbf{K} along with the boundary $\partial\mathbf{K}$ constitute the admissible region for deformation. We define a region Γ where $\Gamma \subset \partial\mathbf{B}_n$ as the part of the boundary that could potentially come into contact with the die. The unit normal to the die is defined such that it always points towards the admissible region. We define a gap function g as the shortest distance between the die surface and a point in space denoted by \mathbf{x} .

$$\bar{\mathbf{y}} - \mathbf{x} = g(\mathbf{x})\boldsymbol{\nu}(\bar{\mathbf{y}}) \quad (6)$$

where $\bar{\mathbf{y}} \in \partial\mathbf{K}$ is the value of \mathbf{y} which minimizes the norm $\|\mathbf{x} - \mathbf{y}\|$. Using the above definition of the gap function, we can now define the impenetrability constraints for the contact between the die and the workpiece. For all $\mathbf{x}_n \in \Gamma$, with $\mathbf{x}_{n+1} = \mathbf{x}_n + \mathbf{u}(\mathbf{x}_n)$,

$$\begin{aligned} g(\mathbf{x}_{n+1}) &\leq 0 \\ \lambda_N &= \boldsymbol{\nu} \cdot \boldsymbol{\lambda} \\ \lambda_N g(\mathbf{x}_{n+1}) &= 0 \end{aligned} \quad (7)$$

where $\boldsymbol{\lambda}$ is the current traction vector defined on Γ and λ_N is its normal component. Assuming that Coulomb friction exists in the contact region with a friction coefficient μ , the Coulomb friction law can be written as follows:

$$\begin{aligned} \Phi &:= \|\boldsymbol{\lambda}_T\| - \mu\lambda_N \leq 0 \\ \mathbf{v}_T^b &:= \dot{\gamma} \frac{\boldsymbol{\lambda}_T}{\|\boldsymbol{\lambda}_T\|} \\ \dot{\gamma} &\geq 0 \\ \dot{\gamma}\Phi &= 0 \end{aligned} \quad (8)$$

In the above equation $\boldsymbol{\lambda}_T = \lambda_{T_\alpha} \boldsymbol{\tau}^\alpha$ is the tangential traction and $\|\boldsymbol{\lambda}_T\| = [\lambda_{T_\beta} m^{\beta\gamma} \lambda_{T_\gamma}]$, where $m^{\beta\gamma} = \boldsymbol{\tau}^\beta \cdot \boldsymbol{\tau}^\gamma$

is the metric tensor. \mathbf{v}_T^b represents the dual of the relative velocity \mathbf{v}_T between the workpiece and the die defined as follows:

$$\mathbf{v}_T = \frac{d}{dt}[\bar{\mathbf{y}}] = \dot{\xi}^\alpha \boldsymbol{\tau}_\alpha \quad (9)$$

where $\bar{\xi}$ is the value of parameter associated with $\bar{\mathbf{y}}$. A unique value of the parameter $\bar{\xi}$ is associated with each $\bar{\mathbf{y}}$. The contact constraints are enforced using an augmented Lagrangian formulation and the time integration of the frictional constraint is achieved by a trial state/return map algorithm. We introduce the Lagrange multipliers λ_N , λ_{T_1} and λ_{T_2} corresponding to the normal and tangential tractions, respectively. The penalty parameters in the normal and tangential directions are denoted by ϵ_N and ϵ_T . The principle of virtual work equation is nonlinear and a Newton-Raphson procedure is used to incrementally solve for the new configuration \mathbf{B}_{n+1} . At every contact iteration, given the new workpiece configuration, the contact constraints are checked for satisfaction. If not satisfied, the Lagrange multipliers are updated and the solution proceeds to the next iteration. Complete details of the algorithm are provided in [7].

3. Formulation of the continuum sensitivity method for a generic forming stage:

We now consider the sensitivities with respect to the design parameters β of field variables in the current forming stage. Such typical process parameters may include the ram speed history, the die surface of the current stage, and others. An updated Lagrangian representation is adopted here. Let us consider a generic field Φ . The parameter sensitivity $\hat{\Phi} = \hat{\Phi}(\mathbf{x}_n, t; \beta)$ is defined as the total Gateaux differential of $\Phi = \hat{\Phi}(\mathbf{x}_n, t; \beta)$ in the direction $\Delta\beta$ computed at β :

$$\hat{\Phi}(\mathbf{x}_n, t; \beta, \Delta\beta) = \frac{d}{d\omega} \hat{\Phi}(\mathbf{X}, t; \beta + \omega\Delta\beta)|_{\omega=0} \quad (10)$$

$$t \in [t_n, t_{n+1}]$$

Extension of these definitions to shape sensitivities (e.g. sensitivities with respect to the preform shape) is described in detail in [1].

The developed sensitivity scheme proceeds as follows. The governing equations of the various sub-problems in the direct analysis (e.g. the kinematic, constitutive, contact and thermal analysis) are first design-differentiated and then appropriate weak forms, time integration and discretization are introduced. The resulting linear sensitivity sub-problems are combined to produce a linear problem for computing the sensitivity of the deformation, plastic deformation gradient and material state. A unified weak form is developed here to compute sensitivities with respect to any design parameter (which maybe a scalar or a vector field).

A weak form for the linear sensitivity analysis of a generic forming stage is identified by considering the sensitivity of the equilibrium equations and boundary conditions at the continuum level. The sensitivity deformation problem is developed on the reference preform \mathbf{B}_n . The design sensitivity of the equilibrium equation (Eq. (4)) at

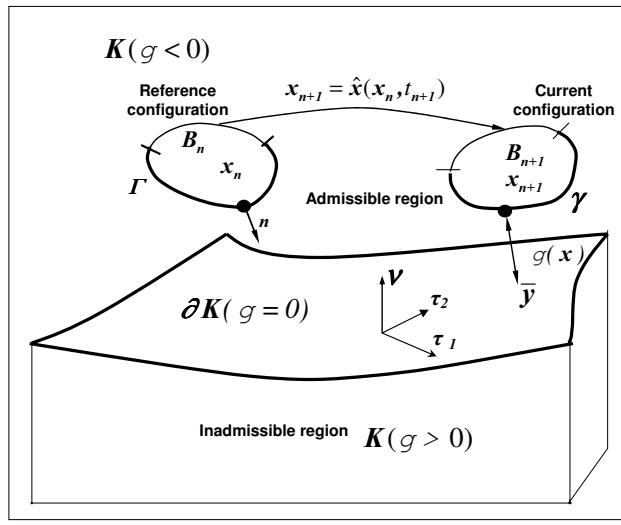


Figure 1: Schematic of the contact problem.

$t = t_{n+1}$ results in:

$$\frac{\overset{\circ}{\circ}}{\nabla_n \cdot \mathbf{P}_r} + \overset{\circ}{\circ} f = 0, \quad \forall \mathbf{x}_n \in B_n \quad (11)$$

A variational form for the above sensitivity equilibrium equation can be posed as follows [3]:

$$\begin{aligned} & \int_{B_n} \overset{\circ}{\circ} \mathbf{P}_r \cdot \nabla_n \tilde{\eta} dV_n - \\ & \int_{B_n} \left(\mathbf{P}_r \left[\nabla_n \cdot \mathbf{L}_n^T \right] \right) \cdot \tilde{\eta} dV_n - \\ & \int_{B_n} \left(\mathbf{P}_r \mathbf{L}_n^T \right) \cdot \nabla_n \tilde{\eta} dV_n = \\ & \int_{\Gamma_n} \left\{ \overset{\circ}{\circ} \boldsymbol{\lambda} - [\mathbf{L}_n \cdot (\mathbf{N} \otimes \mathbf{N})] \boldsymbol{\lambda} \right\} \cdot \tilde{\eta} dA_n \end{aligned} \quad (12)$$

where $\tilde{\eta}$ is a kinematically admissible sensitivity deformation field expressed over the reference configuration B_n , \mathbf{N} is the unit normal vector to Γ_n and the (known) design velocity gradient \mathbf{L}_n at t_n is defined as follows:

$$\mathbf{L}_n \equiv \nabla_n \hat{\mathbf{x}}(\mathbf{x}_{n-1}, t_n; \boldsymbol{\beta}, \Delta\boldsymbol{\beta}) = \overset{\circ}{\circ} \mathbf{F}_n \mathbf{F}_n^{-1} \quad (13)$$

The primary unknown of Eq. (12) is the design differential $\overset{\circ}{\circ} \mathbf{x}_{n+1} = \hat{\mathbf{x}}(\mathbf{x}_n, t_{n+1}; \boldsymbol{\beta}, \Delta\boldsymbol{\beta})$. In order to obtain the final form of the variational sensitivity problem, the relationships between (a) $\overset{\circ}{\circ} \mathbf{F}_r$ and $\overset{\circ}{\circ} \mathbf{x}_{n+1}$ (b) $\overset{\circ}{\circ} \mathbf{P}_r$ and $[\overset{\circ}{\circ} \mathbf{x}_{n+1}, \overset{\circ}{\circ} \theta_{n+1}]$ (c) $\overset{\circ}{\circ} \boldsymbol{\lambda}$ and $\overset{\circ}{\circ} \mathbf{x}_{n+1}$ need to be developed. The relationship between $\overset{\circ}{\circ} \mathbf{F}_r$ and $\overset{\circ}{\circ} \mathbf{x}_{n+1}$ is purely kinematic in nature. The relationship between $\overset{\circ}{\circ} \mathbf{P}_r$ and $[\overset{\circ}{\circ} \mathbf{x}_{n+1}, \overset{\circ}{\circ} \theta_{n+1}]$ is obtained from the sensitivity constitutive problem. The relationship between $\overset{\circ}{\circ} \boldsymbol{\lambda}$ and $\overset{\circ}{\circ} \mathbf{x}_{n+1}$ is obtained from a regularized sensitivity contact problem outlined in the next subsection.

3.1 Three-dimensional sensitivity contact problem:

The sensitivity contact problem involves computing the sensitivities of the contact traction vector which can be written as

$$\begin{aligned} \overset{\circ}{\circ} \boldsymbol{\lambda} = & \overset{\circ}{\circ} \lambda_N \boldsymbol{\nu}(\bar{\mathbf{y}}) + \lambda_N \overset{\circ}{\circ} \boldsymbol{\nu}(\bar{\mathbf{y}}) - \overset{\circ}{\circ} \lambda_{T_1} \boldsymbol{\tau}^1(\bar{\mathbf{y}}) - \lambda_{T_1} \overset{\circ}{\circ} \boldsymbol{\tau}^1(\bar{\mathbf{y}}) \\ & - \overset{\circ}{\circ} \lambda_{T_2} \boldsymbol{\tau}^2(\bar{\mathbf{y}}) - \lambda_{T_2} \overset{\circ}{\circ} \boldsymbol{\tau}^2(\bar{\mathbf{y}}) \end{aligned} \quad (14)$$

where $\overset{\circ}{\circ} \boldsymbol{\tau}^1(\bar{\mathbf{y}})$ and $\overset{\circ}{\circ} \boldsymbol{\tau}^2(\bar{\mathbf{y}})$ are the sensitivities of the dual of the tangent vectors. To allow for the computation of the design derivatives in the equation above, certain regularization assumptions are introduced:

- A particle that lies in the admissible (or inadmissible) region for the direct problem also lies in the admissible (or inadmissible) region for the sensitivity problem.
- A point that is in a state of slip (or stick) in the direct problem is also in the same state in the sensitivity problem.

As a result of the above assumptions, Eq. (14) gives a complete description of the sensitivity contact problem.

The quantities $\overset{\circ}{\circ} \lambda_N$, $\overset{\circ}{\circ} \lambda_{T_1}$, $\overset{\circ}{\circ} \lambda_{T_2}$, $\overset{\circ}{\circ} \boldsymbol{\tau}^1(\bar{\mathbf{y}})$, $\overset{\circ}{\circ} \boldsymbol{\tau}^2(\bar{\mathbf{y}})$ and $\overset{\circ}{\circ} \boldsymbol{\nu}(\bar{\mathbf{y}})$ depend on the sensitivities of the closest point projection $[\overset{\circ}{\circ} \xi^1, \overset{\circ}{\circ} \xi^2]$, and the sensitivity of the gap function $\overset{\circ}{\circ} g$ which in turn depend on the sensitivity of the displacements $\overset{\circ}{\circ} \mathbf{x}$. The sensitivity of the tangent vector takes the form,

$$\begin{aligned} \overset{\circ}{\circ} [\boldsymbol{\tau}^\alpha] & = \overset{\circ}{\circ} [\boldsymbol{\tau}^\alpha(\bar{\mathbf{y}})] = \overset{\circ}{\circ} [\bar{\mathbf{y}}_{,\xi^\alpha}] = \overset{\circ}{\circ} \bar{\mathbf{y}}_{,\xi^\alpha} + \bar{\mathbf{y}}_{,\xi^\alpha, \xi^\alpha} \overset{\circ}{\circ} \xi^\alpha \\ & + \bar{\mathbf{y}}_{,\xi^\alpha, \xi^\beta} \overset{\circ}{\circ} \xi^\beta \quad (\text{no sum on } \alpha, \beta) \end{aligned} \quad (15)$$

The sensitivity of the dual of the tangent vector can be obtained from the above by the following expression

$$\overset{\circ}{\boldsymbol{\tau}^\alpha} = m^{\alpha\beta} \overset{\circ}{\boldsymbol{\tau}^\beta} + \overset{\circ}{m}^{\alpha\beta} \boldsymbol{\tau}^\beta \quad (16)$$

where $m^{\alpha\beta}$ denotes the sensitivity of the metric tensor $m^{\alpha\beta} = \boldsymbol{\tau}^\alpha \cdot \boldsymbol{\tau}^\beta$ in the given coordinate system. The sensitivity of the normal vector can be written as,

$$\overset{\circ}{\boldsymbol{\nu}} = \overset{\circ}{[\boldsymbol{\nu}(\boldsymbol{y})]} = \frac{\overset{\circ}{\boldsymbol{\tau}_1 \times \boldsymbol{\tau}_2}}{\|\overset{\circ}{\boldsymbol{\tau}_1 \times \boldsymbol{\tau}_2}\|} \quad (17)$$

The remaining quantities $\overset{\circ}{\lambda}_N$, $\overset{\circ}{\lambda}_{T_1}$ and $\overset{\circ}{\lambda}_{T_2}$ are computed by considering the constraints that are used for evaluating the quantities λ_N , λ_{T_1} and λ_{T_2} in the direct deformation problem. Similar to the direct problem, $\overset{\circ}{\lambda}_N$, $\overset{\circ}{\lambda}_{T_1}$ and $\overset{\circ}{\lambda}_{T_2}$ can be thought of as the Lagrange multipliers for the sensitivity problem. To enforce the normal contact constraints in the sensitivity problem the following penalization is used:

$$\overset{\circ}{\lambda}_N = \overset{\circ}{\lambda}_{N_n} + \epsilon_{N_s} \overset{\circ}{g}_{n+1} \quad (18)$$

where $\overset{\circ}{\lambda}_{N_n}$ is the normal traction sensitivity calculated in the previous time step and ϵ_{N_s} is the normal penalty used in the sensitivity problem to enforce the normal constraints. In the developed formulation, the normal penalty in the sensitivity problem is not of the same value as the normal penalty in the direct problem. A discussion on this issue is presented at the end of the subsection. To enforce the tangential contact constraints for sticking the following penalization is used:

$$\overset{\circ}{\xi}_\alpha = \frac{1}{\epsilon_{T_s}} \overset{\circ}{\lambda}_{T_\alpha} \quad (19)$$

which on integration leads to

$$\overset{\circ}{\lambda}_{T_\alpha} = \overset{\circ}{\lambda}_{T_{n_\alpha}} + \epsilon_{T_s} (\overset{\circ}{\xi}_\alpha - \overset{\circ}{\xi}_{n_\alpha}), \quad \alpha = 1, 2 \quad (20)$$

where $\overset{\circ}{\lambda}_{T_{n_\alpha}}$ and $\overset{\circ}{\xi}_{n_\alpha}$ are known from the previous time step. Similar to the normal penalty, the tangent penalty in the sensitivity problem ϵ_{T_s} differs from that in the direct problem. For sliding contact, $\overset{\circ}{\lambda}_{T_\alpha}$ is calculated from the expression

$$\overset{\circ}{\lambda}_{T_\alpha} = \left(\frac{\overset{\circ}{\lambda}_{T_\alpha}^{trial}}{\mu \lambda_N \|\overset{\circ}{\boldsymbol{\lambda}_T}\|} \right), \quad \alpha = 1, 2 \quad (21)$$

The above term can be written as

$$\overset{\circ}{\lambda}_{T_\alpha} = \mu \overset{\circ}{\lambda}_N \frac{\overset{\circ}{\lambda}_{T_\alpha}^{trial}}{\|\overset{\circ}{\boldsymbol{\lambda}_T}\|} + \mu \lambda_N \frac{\overset{\circ}{\lambda}_{T_\alpha}^{trial}}{\|\overset{\circ}{\boldsymbol{\lambda}_T}\|} + \mu \lambda_N \lambda_{T_\alpha}^{trial} \left(\frac{\overset{\circ}{1}}{\|\overset{\circ}{\boldsymbol{\lambda}_T}\|} \right) \quad (22)$$

An important point to be noted here is the presence of the term $\lambda_{T_\alpha}^{trial}$, which is the trial tangent traction calculated in the radial return mapping scheme in the direct problem,

i.e. the sensitivity of the traction term depends on the trial traction and not just on the current traction value. The sensitivity of the trial traction term can be expressed as follows:

$$\overset{\circ}{\lambda}_{T_\alpha}^{trial} = \overset{\circ}{\lambda}_{T_{n_\alpha}} + \epsilon_T (\overset{\circ}{\xi}_\alpha - \overset{\circ}{\xi}_{n_\alpha}), \quad \alpha = 1, 2 \quad (23)$$

After some intensive mathematical manipulations, the above contact traction sensitivities can be expressed concisely as follows:

$$\overset{\circ}{\boldsymbol{\lambda}} = \zeta_1 \overset{\circ}{g} + \zeta_2 \overset{\circ}{\xi}^1 + \zeta_3 \overset{\circ}{\xi}^2 + \zeta_4 \quad (24)$$

The linear relationship between $\overset{\circ}{\xi}^1, \overset{\circ}{\xi}^2$ and $\overset{\circ}{x}$ can be developed by considering the sensitivity of the expression $(\boldsymbol{y} - \boldsymbol{x}) \cdot \boldsymbol{\tau}_\alpha(\boldsymbol{y}) = 0$.

The relationship between $\overset{\circ}{g}$ and $\overset{\circ}{x}$ can be developed by design differentiation of Eq. (6).

In this subsection, the sensitivity contact problem was presented in a continuum contact sensitivity setting. An alternate formulation can be considered where the design-differentiation of the corresponding discrete equations used in the augmented Lagrangian analysis in the direct contact sub-problem is carried out. However, this interpretation requires that the penalty parameters be identical in both the direct and sensitivity contact sub-problems. Such a restriction is unnecessary as it implies that the magnitude of the penalty parameters in the sensitivity contact analysis is limited by corresponding values used in the direct contact problem. In the direct contact problem, to prevent ill-conditioning of the non-linear system of equations an augmented Lagrangian approach was used and thus the penalties were smaller compared to that of a direct penalty approach. Since the sensitivity problem is linear, use of larger penalties is possible. Thus to avoid augmentations to the Lagrange multipliers in the sensitivity problem, we compute the sensitivities of the contact tractions in one step by using oversized penalties.

4. Applications: We now proceed to validate the sensitivity algorithm and discuss design applications. In all the problems structured meshes comprising of 8-noded brick elements are used. No remeshing operations have been performed. The kinematics are stabilized using the F-bar assumed strain method with a stabilization parameter $\epsilon = 1e - 3$ which is discussed in detail in [2]. The workpiece material is 1100-Al with initial temperature of 673K. The constitutive model and material properties used are identical to those in [4]. In the last example the workpiece material is assumed to be Fe-2%Si. The constitutive model for this material is given in [5].

4.1 Sensitivity comparisons: To validate the continuum sensitivity algorithm, we consider the benchmark problem of flat die forging of a cylinder and compare the sensitivities obtained using the forward difference form of the finite difference method (FDM) and the continuum sensitivity method (CSM). The initial height and the radius of the preform are taken as 3.0 mm and 1.0 mm, respectively. The forging rate is taken as 0.01 mm/s. The

stroke is fixed at 1.0 mm, which corresponds to a total deformation of 33%. The die is assumed to be isothermal, while the workpiece is non-isothermal. Using symmetry conditions only one-eighth of the domain is used for computation. A mesh consisting of 750 elements and 1001 nodes was used. Neumann boundary conditions are assumed at the symmetry planes and convective and radiative boundary conditions are assumed at the free surfaces of the preform. The coupling tolerance between the thermal and the deformation problems is taken as $1e-4$ [4]. The energy and displacement error norms for satisfying convergence in the nonlinear iterations in the direct problem are each taken as $1e-5$, whereas the normal and tangent penalties for the contact problem are taken as $1e5$. The normal and tangent penalties for the sensitivity contact problem are taken as $1e7$. A friction coefficient of 0.4 is assumed at the die workpiece interface. Using this problem as the reference state, various sensitivities are computed.

For computing the shape sensitivities, the curved surface of the preform is parameterized and constrained such that it can at the most have an elliptical cross-section. The semi-major axis $a(\alpha)$ and semi-minor axis $b(\alpha)$ of the ellipse are each modeled using degree 6 Bézier curves using the restriction that $x'(0) = 0$ and $y'(0) = 0$, ($\alpha = 0$ corresponds to the mid plane of the cylinder). Thus the design shape parameters for a shape sensitivity problem can be defined as

$$\beta = \{\beta_1, \beta_2, \beta_3, \beta_4, \beta_5, \beta_6, \beta_7, \beta_8, \beta_9, \beta_{10}, \beta_{11}, \beta_{12}\}^T$$

The shape sensitivities are computed with a perturbation of $1e-4$ to β_3 . The CSM sensitivities are compared with the FDM sensitivities in Figs. 2-3. As can be observed, the sensitivities compare extremely well. Since the CSM involves solution of one nonlinear direct problem and one linear sensitivity problem for each design variable, it is relatively much faster than the FDM which requires solving an additional nonlinear direct problem for each design variable.

4.2 Extrusion die design for uniform material state:

We consider an extrusion process with a fixed reduction in cross-section over a fixed length. The objective is to design the die shape such that the state variable distribution (isotropic material hardening behavior) at the exit is as uniform as possible. The extrusion die is defined and parameterized as follows:

$$\begin{aligned} & \text{shape}(\xi^1, \xi^2) = \\ & \begin{cases} x(\xi^1, \xi^2) = \sum_{i=0}^6 \beta_{i+1} \Phi_i(\xi^1) \cos(\xi^2 \frac{\pi}{2}) \\ y(\xi^1, \xi^2) = \sum_{i=0}^6 \beta_{i+1} \Phi_i(\xi^1) \sin(\xi^2 \frac{\pi}{2}) \\ z(\xi^1, \xi^2) = \xi^1/2 \end{cases} \quad (25) \end{aligned}$$

where $\Phi_i(\xi^1)$ are degree 6 Bernstein polynomials. The parameters β_1 and β_7 are taken as 0.5 and 0.43 mm, respectively which results in a 26% reduction in the cross-sectional area over a length of 0.5 mm. The die curvature at the entrance and the exit is taken to be perpendicular to the radius by assuming $\beta_1 = \beta_2$ and $\beta_6 = \beta_7$. Only the parameters $\beta_3, \beta_4, \beta_5$ are allowed to vary. As a result, the CSM design problem to be solved involves one direct problem and only 3 sensitivity problems. The initial

billet is a cylinder of radius 0.5 mm and height 2 mm. Using symmetry only one-fourth of the domain is used. A mesh consisting of 540 elements and 777 nodes is used in the analysis. The extrusion process is carried out with a velocity of 0.01 mm/s and a die-workpiece friction coefficient of 0.01. Other simulation parameters are the same as in the previous example. Steady state conditions are reached after a time of 105 s. The objective function for this problem can be defined as

$$\min_{\beta} F(\beta) = \sum_{i=1}^N w_i (s_i(\beta) - \bar{s}(\beta))^2 \quad (26)$$

where w_i are the weights and s_i ($i = 1 \dots N$) are the corresponding state variable values at the exit cross section ($z = 0.5$) chosen to carry out the area integration and $\bar{s} = \frac{\sum_{i=1}^N w_i s_i}{\sum_{i=1}^N w_i}$.

The initial guess for the optimization problem is taken as $\beta_3 = 0.4825, \beta_4 = 0.465, \beta_5 = 0.4475$ which gives a linear interpolation of the control points between 0.5 and 0.43. The optimal solution is obtained in 8 iterations. The objective function is plotted in Fig. 4. The final optimal design parameters are obtained as $\beta_3 = 0.45021, \beta_4 = 0.44412, \beta_5 = 0.44125$. The state variable distribution at the exit for the initial and final iterations are shown in Figs. 5-6, respectively. As can be seen, a considerable reduction in the deviation of the state variable at the exit is achieved by a change in the three design parameters considered.

4.3 Preform design to fill the die cavity for a porous material:

In this problem, the forging of a circular disc is considered (Fig. 7). The objective is to design the preform of variant volume for a final forged product (with fixed stroke) such that the die cavity is fully filled. The workpiece material considered is made of a porous Fe-2%Si with an initial void fraction of 5%. The constitutive model for the above material is outlined in [5]. As a result of the porosity, the volume of the material changes when it is subjected to deformation. In the regions where there are compressive stresses, the void fraction decreases leading to a decrease in volume. The converse happens in regions of tensile stresses. Thus this problem involves not only estimating the optimum preform shape but also the optimum initial volume such that the die cavity is filled. One way to ensure that the die cavity is filled is to consider a preform of a much larger volume than that needed. In this case, the die cavity is filled up but there will be considerable material wastage due to flash.

The design objective in this example is thus posed as computing the optimum preform shape and its volume which fills the die cavity with minimum flash for the given die stroke. The optimization iterations start with a preform of slightly lesser volume than the die cavity and the design iterations try to attain the optimum volume and shape of the final preform which fills the die cavity with minimum flash. The initial preform is assumed to be a cylinder of radius 1.0 mm and height 1.44 mm. The preform is subjected to a total deformation of 58% (height reduction from 1.44 mm to 0.6 mm at the center). The

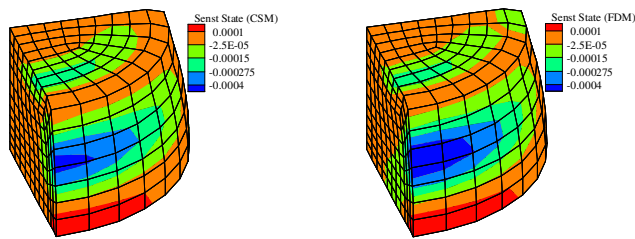


Figure 2: Comparison of the shape sensitivities using CSM and FDM for the scalar state variable (represents the isotropic material hardening behavior).

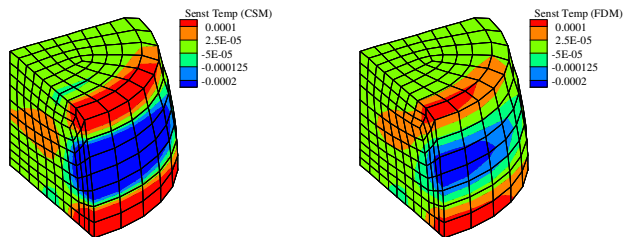


Figure 3: Comparison of the shape sensitivities using CSM and FDM for the workpiece temperature.

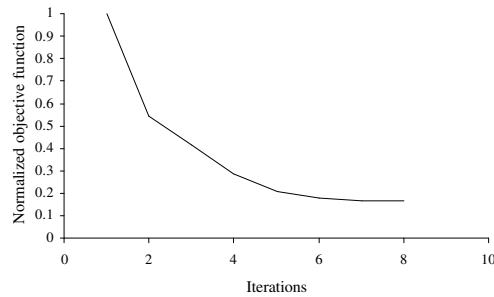


Figure 4: Normalized objective function variation for the extrusion problem.

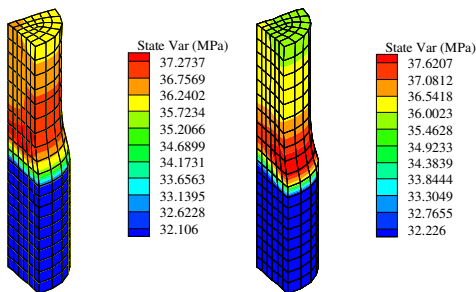


Figure 5: State variable distribution at steady-state for the initial and final optimization iterations.

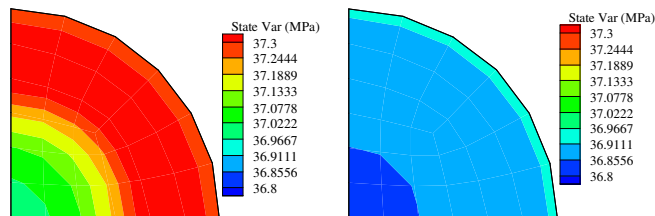


Figure 6: State variable distribution at the exit cross section for the initial and final optimization iterations.

workpiece is isothermal with a constant temperature of 1273 K. The friction coefficient is assumed to be 0.1. Using symmetry, only one-eighth of the domain is used for computations. A mesh consisting of 600 elements and 819 nodes is used in this simulation. The curved surface parameterization for the preform is the same as in Example 1. The energy and displacement error norms are the same as in the previous examples. The normal and tangent penalties in the direct problem are taken as 10^5 and 10^4 , respectively. The normal and tangent penalties in the sensitivity problem are taken as 10^7 and 10^6 , respectively. The forging velocity is taken as 0.01mm/s. For this optimization problem, the objective function is defined as follows:

$$\min_{\beta} F(\alpha) = \frac{1}{2N} \sum_{i=1}^N \{(x_i(\beta) - x_i^{desired})^2 + (y_i(\beta) - y_i^{desired})^2 + (z_i(\beta) - z_i^{desired})^2\} \quad (27)$$

where $x_i^{desired}$, $y_i^{desired}$ and $z_i^{desired}$ are the closest point projections of the points $x_i(\beta)$, $y_i(\beta)$, $z_i(\beta)$ on the die and N denotes the number of points on the contact boundary. Thus the objective is to minimize the gap between the preform and corresponding closest point on the die.

Figure 7 shows the guess preform and the final forged product for the first optimization iteration. The optimal solution for the design problem is attained in 5 iterations. The optimal preform shape and the final forged product are shown in Fig. 8. The volume of the optimum preform is 5.305 mm^3 , and the volume of the final forged product is 5.205 mm^3 . The volume of the die cavity is 5.104 mm^3 . The objective function for the optimization problem is plotted in Fig. 9. The state variable (isotropic scalar resistance), void fraction and plastic strain distribution in the optimal forged product are shown in Fig. 10.

5. Summary and research activities in progress: This paper presented some early results and theoretical foundations of a 3D metal forming design simulator being developed at our laboratory. The initial results show great potential for extension to realistic large-scale 3D applications. Our current research efforts are concentrated in the following areas:

- Extension of the design simulator to complicated multi-stage forgings. The key step in accomplishing this objective lies in incorporating remeshing and suitable data transfer schemes which is our current area of priority. Efforts are also under way to increase the scalability of the design simulator using the parallel toolbox PetSc [8].
- Development of a multiscale version of the design simulator employing a polycrystal plasticity based constitutive model. This involves a novel two length scale sensitivity analysis for process and materials design. Initial results were presented in [9].
- We have also initiated efforts to account for uncertainty in metal forming and large deformation

processes in general. A novel spectral method has been developed for this purpose in our laboratory [10]-[12]. Some early results of this work have been presented in [13] which considers uncertainty in initial configuration, processing conditions and heterogeneous material properties. Extensions of the above to stochastic upscaling of properties from atomistic and microstructure scales to the macro scale for a realistic assessment of material behavior is being actively pursued.

- Using data-mining techniques, we have demonstrated the ability to select processing information from databases of microstructural information in the form of orientation distribution functions [14]. Further, these techniques have been used for microstructure reconstruction and representation using databases of microstructures [15, 16]. By combining multi-scale computational algorithms with ideas drawn from fields such as databases, machine learning, statistics, machine vision and parallel computing, we aim to generate an integrated approach to knowledge discovery for the design of optimized materials.

6. Acknowledgements: The work presented here is funded by the Engineering Design Division of DMI of the National Science Foundation (grant DMI-0113295). Additional support was provided by the Computational Mathematics program of the Air Force Office of Scientific Research (grants F49620-00-1-0373 and FA9550-04-1-0070) and the Army research office (grant W911NF-04-1-0283). The computing for this project was supported by the Cornell Theory Center. In addition to Swagato Acharjee, other graduate students from our laboratory partially supported under this grant include S. Ganapathysubramanian, V. Sundararaghavan, V. A. Badri Narayanan, S. Sankaran and J. Wang.

References

- [1] A. Srikanth and N. Zabarar, "Shape optimization and preform design in metal forming", *Computer Methods in Applied Mechanics and Engineering*, Vol. 190, pp. 1859–1901, 2000.
- [2] N. Zabarar and A. Srikanth, "An object-oriented programming approach to the Lagrangian FEM analysis of large inelastic deformations and metal forming processes", *International Journal for Numerical Methods in Engineering*, Vol. 45, pp. 399–445, 1999.
- [3] N. Zabarar, Y. Bao, A. Srikanth and W. G. Frazier, "A continuum sensitivity analysis for metal forming processes with application to die design problems", *International Journal for Numerical Methods in Engineering*, Vol. 48, pp. 679–720, 2000.
- [4] S. Ganapathysubramanian and N. Zabarar, "A continuum sensitivity method for finite thermo-inelastic deformations with applications to the design of hot

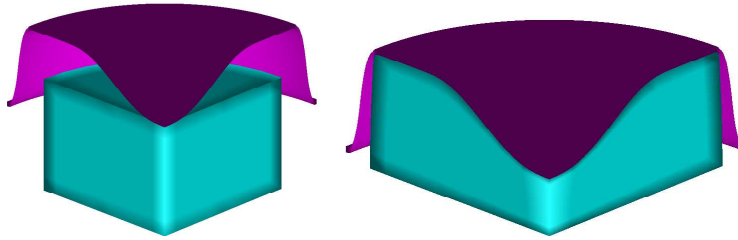


Figure 7: Initial preform and final forged product for the closed die forging problem (Example 3).

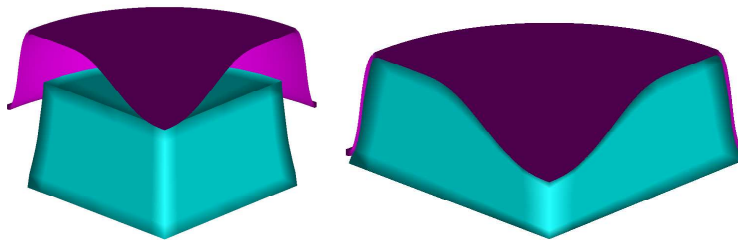


Figure 8: Optimal preform and final forged product for the closed die forging problem.

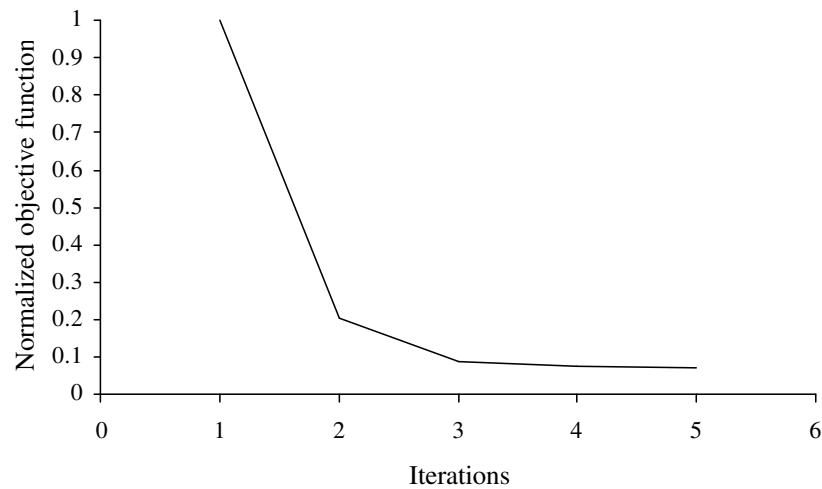


Figure 9: Normalized objective function variation for the closed die forging problem.

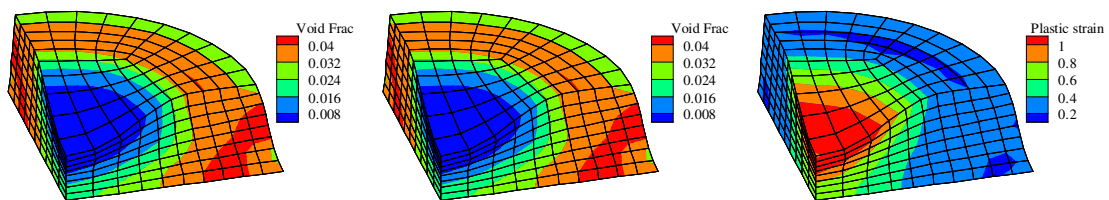


Figure 10: Void fraction, state variable (isotropic scalar resistance) and plastic strain distribution in the optimum forged product.

- forming processes”, *International Journal for Numerical Methods in Engineering*, Vol. 55, pp. 1391–1437, 2002.
- [5] S. Ganapathysubramanian and N. Zabaras, “Computational design of deformation processes for materials with ductile damage”, *Computer Methods in Applied Mechanics and Engineering*, Vol. 192, pp. 147–183, 2003.
- [6] T.A. Laursen, *Computational contact and impact mechanics -Fundamentals of modeling interfacial phenomena in nonlinear finite element analysis*, Springer, Berlin, 2002.
- [7] Swagato Acharjee and N. Zabaras, “The continuum sensitivity method for the computational design of three-dimensional deformation processes”, *Computer Methods in Applied Mechanics and Engineering*, in press.
- [8] Satish Balay, Kris Buschelman, Victor Eijkhout, D. Gropp, Dinesh Kaushik, Matthew G. Knepley, Lois Curfman McInnes, Barry F. Smith and Hong Zhang, “PETSc Users Manual”, Argonne National Laboratory, 2004.
- [9] S. Ganapathysubramanian and N. Zabaras, “Modeling the thermoelastic-viscoplastic response of polycrystals using a continuum representation over the orientation space”, *International Journal of Plasticity*, in press.
- [10] Velamur Asokan Badri Narayanan and N. Zabaras, “Stochastic inverse heat conduction using a spectral approach”, *International Journal for Numerical Methods in Engineering*, Vol. 60/9, pp. 1569-1593, 2004.
- [11] Velamur Asokan Badri Narayanan and N. Zabaras, “Variational multiscale stabilized FEM formulations for transport equations: stochastic advection-diffusion and incompressible stochastic Navier-Stokes equations”, *Journal of Computational Physics*, in press.
- [12] V. A. Badri Narayanan and N. Zabaras, “Using stochastic analysis to capture unstable equilibrium in natural convection”, *Journal of Computational Physics*, submitted for publication.
- [13] S. Acharjee and N. Zabaras, “Uncertainty propagation in finite deformation plasticity – A spectral stochastic Lagrangian approach”, *Computer Methods in Applied Mechanics and Engineering*, submitted for publication.
- [14] V. Sundararaghavan and N. Zabaras, “On the synergy between classification of textures and deformation process sequence selection”, *Acta Materialia*, submitted for publication.
- [15] V. Sundararaghavan and N. Zabaras, “A dynamic material library for the representation of single phase polyhedral microstructures”, *Acta Materialia*, Vol. 52/14, pp. 4111-4119, 2004.
- [16] V. Sundararaghavan and N. Zabaras, “Classification of three-dimensional microstructures using support vector machines”, *Computational Materials Science*, in press.